Title

Atom-at-a-Time Radioactive Molecule Identification: Looking toward Studies of Superheavy Elements

Journal

The Journal of Physical Chemistry A, 129(29)

ISSN

1089-5639

Authors

Garcia, FatimaH
Pore, Jennifer L
Gates, Jacklyn M
et al.

Publication Date

2025-07-24

DOI

10.1021/acs.jpca.5c02098

Peer reviewed

Atom-at-a-time Radioactive Molecule Identification: Looking Toward Studies of Superheavy Elements

Fatima H. Garcia[1], Jennifer L. Pore[1,2*], Jacklyn M. Gates[1,2], Heather L. Crawford[1], Alexander Ditter[2], Paul Fallon[1], John K. Gibson[2], John Gooding[1,3], Mallory McCarthy[2,3], Rodney Orford[1], Ziad Shafi[2,4], David K. Shuh[2], Mark A. Stoyer[5]

[1]Nuclear Science Division, Lawrence Berkeley National Laboratory, Berkeley, CA, 94720.
[2]Chemical Sciences Division, Lawrence Berkeley National Laboratory, Berkeley, 94720, CA.
[3]Department of Nuclear Engineering, UC Berkeley, Berkeley, 94720, CA.
[4]Department of Chemistry, UC Berkeley, Berkeley, 94720, CA.
[5]Nuclear and Chemical Science Division, Lawrence Livermore National Laboratory, Livermore, CA 94550.

*Corresponding author(s). E-mail(s): jpore@lbl.gov;

Abstract

The chemical behavior of superheavy elements (SHEs, $Z > 103$) remains poorly understood. Their chemical properties are expected to deviate from established periodic trends, challenging the predictive power of the periodic table. To investigate these elements experimentally, they must first be synthesized through nuclear reactions and then quickly subjected to chemical studies before they decay. Given the low production rates of these reactions and the need for measurements on an atom-at-a-time basis, innovative techniques are needed. To address these challenges, a novel gas-phase chemistry method has been developed at Lawrence Berkeley National Laboratory, utilizing the Berkeley Gas-filled Separator and FIONA. This technique enables the production, identification, and study of molecular species formed by SHEs. As a proof of concept, we present measurements on the formation and identification of $^{151,152}HoO^{+}$ molecules, demonstrating the capability to study the production of radioactive molecules under controlled conditions and directly identify them via their mass-to-charge

ratio. These measurements validate the effectiveness of this technique for low-statistics SHE studies, highlighting the the potential of this approach to ignite the next generation of experimental SHE chemistry research, offering a path to reevaluate SHE placement on the Periodic Table.

1 Introduction

The study of superheavy elements (SHEs, $Z > 103$) represents a fascinating frontier in experimental and theoretical chemistry [1], driven by the expectation that their chemical behavior may diverge significantly from lighter elements due to pronounced relativistic effects [2, 3]. These deviations raise questions about whether the traditional arrangement of the Periodic Table remains appropriate. However, the current evidence is insufficient to fully assess the impact of these effects or to justify a reorganization of the table. In general, experimental studies of SHEs face significant challenges. These elements are not naturally occurring and must be synthesized one-atom-at-a-time through nuclear reactions. Production rates are exceptionally low, with elements like Rf ($Z = 104$) produced at rates of approximately one per minute [4], and rarer elements, such as Og ($Z = 118$), produced at a rate on one every ten days or less[5]. Then, if a chemical study is to be performed, it must be conducted immediately after synthesis, typically within one second or faster, before the SHE undergoes radioactive decay.

To date, studies of SHE molecule formation and chemical reactivity have predominantly relied on qualitative approaches. Techniques such as ion exchange, liquid-liquid extraction, and gas chromatography have been employed to compare the behavior of SHEs with their lighter homologues [6]. However, these methods have not enabled the direct identification of chemical species, and are heavily reliant on assumptions about their composition. For example, reports of $Sg(CO)_6$ ($Z = 106$) [7] and HsO_4 ($Z = 108$) [8] production are based on inferred properties derived from comparisons with lighter homologues. Such assumptions risk masking the unique impacts of relativistic effects on SHE chemistry. The absence of direct molecular identification may also account for the inconsistencies observed in gas-phase chromatography studies of flerovium (Fl, $Z = 114$) [9, 10, 11]. In multiple experiments, Fl has simultaneously displayed contradictory behavior. In these studies, Fl appeared to act both as a noble gas and as a volatile metal, with two distinct deposition patterns at different temperatures on gold surfaces. It is perhaps more conceivable that Fl forms molecular species during these experiments, potentially explaining its dual characteristics. To advance the field of SHE chemistry, it is imperative to accurately identify the molecular species being studied. This underscores the pressing need for innovative experimental techniques that can directly determine the formation of SHE molecules and provide critical insights into their unique chemical behaviors.

Presently, pursuing further gas-phase chemical studies of SHEs offers significant advantages to extracting fundamental chemical behavior compared to condensed phase studies, as these measurements eliminate confounding effects from aggregation, solvation, or counterions from condensed phase studies [12, 13]. A substantial amount

of gas-phase research has been conducted on main-group elements, lanthanides, and early actinides [14, 15, 16]. For these elements, the energies of electronic configurations have often been measured using laser spectroscopy [17], enabling a deeper understanding of reaction mechanisms leading to the formation of specific molecular species. For instance, a systematic study of lanthanide (Ln) cations reacting with N_2O at room temperature demonstrated that the formation of LnO^+ only occurred when a d^1s^1 electronic configuration was energetically accessible [18]. The reaction rate for LnO^+ formation correlated directly with the energy required to promote an electron from the $4f^n5d^06s^1$ ground state to the $4f^{n-1}5d^16s^1$ excited configuration. Remarkably, this study predicted the promotion energy for Ho^+ ($Z = 67$) with an accuracy of $<$ 0.5 eV before it was measured by laser spectroscopy [19]. These robust and systematic gas-phase methodologies have now established a strong foundation for the future of SHE research. By applying these approaches, it will be possible to investigate chemical reactions with well-understood mechanisms, unlocking critical insights into the availability and energetics of electronic configurations in SHEs, potentially informing a reevaluation of their placement on the periodic table.

Currently, a new gas-phase chemistry technique has been developed at Lawrence Berkeley National Laboratory's (LBNL) 88-Inch Cyclotron Facility, utilizing the Berkeley Gas-filled Separator (BGS) [20] and For the Identification Of Nuclide A (FIONA) [21] experimental devices. With this setup, it is possible to separate, trap, and study the chemical properties of SHE ions produced in nuclear-fusion reactions [22]. While ions of SHE are trapped, they can be exposed to reactive gases such that a chemical reaction could occur, potentially producing molecular species. A huge advantage of this technique is that once molecular species are formed, the identity and quantity can then be directly confirmed with mass-to-charge ratio (A/q) measurements. This technique could allow for the first ever direct identification of SHE molecule formation. In looking towards that goal, this article reports on the study of radioactive Ho isotopes, produced one atom-at-a-time and then exposed to O_2, such that HoO^+ molecules could be formed and directly identified with A/q measurements. Different combinations of reaction times and gas flow rates were used to demonstrate that reaction rates for the formation of molecular species could be measured and to validate this technique for low-statistics measurements of SHEs.

2 Experimental Details

The LBNL 88-Inch Cyclotron Facility has an established Heavy Element program that continues to drive the field forward with new experimental techniques and discoveries [21, 24]. Presently, experiments are performed with the BGS and FIONA devices (schematic is shown in Figure 1). For these studies, ^{151,152}Ho isotopes were produced in the nuclear fusion evaporation reaction $^{40}Ar + {}^{nat}In$. The $^{40}Ar^{8+}$ ion beam was produced by the Advanced Electron Cyclotron Resonance Ion Source (AECR) [25] and accelerated to a lab-frame energy of 160 MeV by the 88-inch cyclotron. The beam then impinged onto a circular (5" diameter) indium target wheel, which rotated at ∼30 Hz. The target was composed of 4 segments of 2 μm self-supporting 99.8% natural indium foils. To monitor the integrated beam on target rate, two silicon pin diode detectors

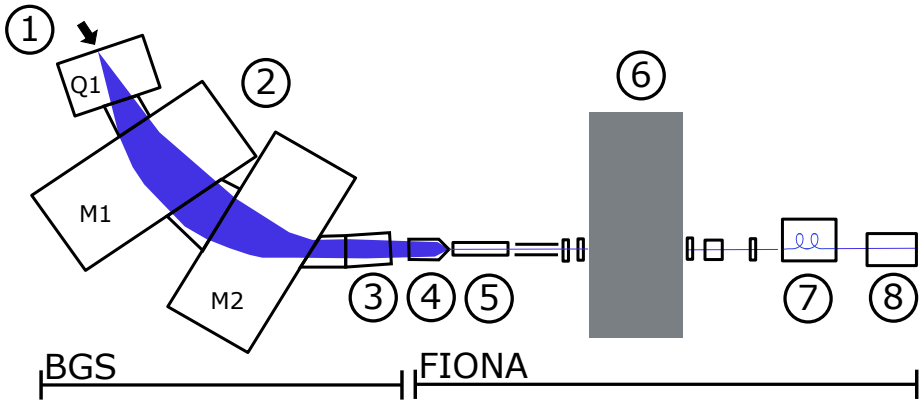

Fig. 1: A schematic of the Berkeley Gas Filled Separator and FIONA experimental set-up. (1) The target position. (2) The three magnets of the BGS; Q1 is a quadrupole, while M1 and M2 are dipoles, used for separating the ions of interest from contaminants. (3) BGS focal plane detector box. (4) Gas catcher, used to thermalize and focus the ions. (5) RFQ trap, used for chemistry experiments. (6) Shielding wall, separating the high- and low-background regions. (7) Trochoidal spectrometer, used for mass identification. (8) Decay station detector box. Adapted from Ref. [23]. Copyright [2021] American Chemical Society.

are positioned downstream of the target wheel at angles of $\pm 27.2^{\circ}$ relative to the beam axis. The observed intensity of scattered beam particles from the target, subsequently referred to as the Rutherford rate, was used to normalize the data to account for any fluctuations in beam current and target thickness that might have occurred between measurements.

Immediately following their production in the nuclear reaction, the Ho isotopes were in a wide range of charge states as they entered the BGS. The BGS was filled with ∼0.5 torr ultrapure He gas, enabling charge exchange to occur to reduce the Ho ions into a more normalized charge state (+5, +6), within the first few mm of their trajectory. In traversing the BGS, the Ho isotopes were then separated from unreacted beam and reaction byproducts based on their magnetic rigidity prior to entering FIONA for chemical studies. FIONA allows for the experimental determination of A/q. A detailed description of FIONA is given in Ref. [21]. In short, FIONA is composed of four major components: a gas catcher, a radiofrequency quadrupole (RFQ) trap, a trochoidal spectrometer and a terminal detector station. The gas catcher, containing ∼150 torr of ultrapure He gas, serves to cool the incoming ions as they undergo further charge exchange and reduction of charge state. Here, ^{151,152}Ho isotopes assumed a 1^{+} charge state. After exiting the gas catcher, the ions entered a RF quadrupole (RFQ) cooler-buncher ion trap, maintained at a pressure of $\sim 10^{-3}$ torr, with three stages of differential pumping to remove the helium gas exiting the gas catcher from the region. Here, the ions were further cooled to near thermal energies, by collisions

with a dilute amount of He gas, and confined in a $\sim$ 1 mm^3 three-dimensional space, through the use of an axial DC potential well and a confining RF field.

The containment of ions within the RFQ trap can be considered analogous to holding them in a beaker, enabling potential chemical studies. Previous work has demonstrated that controlled chemical reactions can be conducted using FIONA, as evidenced by the reduction of Lr^{2+} ions upon exposure to O_2 gas within the RFQ trap [23]. Similarly, in this study, Ho^+ ions were confined within the RFQ trap while O_2 reactive gas was introduced, facilitating the formation of HoO^+.

$$^{151,152}Ho^+ + O_2 \longrightarrow {}^{151,152}HoO^+ + O^* \tag{1}$$

This chemical reaction, shown in Eqn. 1, was studied with different combinations of trapping time and O_2 flow rate to determine the reaction rate of formation. Note that the reaction time here is the amount of time the trap is 'open' for incoming ions to enter and be exposed to the reactive gas, so it is in actuality the maximum exposure time possible. The selected trapping times were 50 and 100 ms, and flow rates of 5×10^{-5}, 1×10^{-4} and 5×10^{-4} mbarL/s were used. Relative pressures of O_2 gas were monitored with the use of a Residual Gas Analyzer (RGA).

At the end of each trapping cycle, the RFQ trap potentially contains leftover reactant ions and a distribution of different reactant products. Upon ejection, this broad distribution of species were then re-accelerated to low energies ($\sim$4 keV) into a low-background area where A/q separation occurs and final detection is performed. Here, A/q separation, was achieved with the use of a trochoidal spectrometer that containing crossed electric and magnetic fields [26]. The trajectories traced by ions (or molecular ions) in this field combination is velocity dependent, meaning that species of different A/q take slightly different paths through the spectrometer and mass separation can be achieved. The mass-separated species are then sent to a Double-sided Silicon Strip Detector (DSSD) at the decay station, where the position of detection of the observed signature-α decay of the species is then correlated to its A/q. To calibrate A/q sensitivity to detection position, ions of a known mass were first sent through and detected in a specific position with FIONA. These nuclides are identified based on their alpha decay properties. Then FIONA can be tuned to a new mass, such that the new mass takes the same trajectory through FIONA, terminating in the same detection position as the calibrated mass. In these measurements, the bare $^{151,152}Ho^+$ ions served as the calibration ions. The A/q calibration procedure is discussed in detail in Ref. [26].

The decay station detector was composed of 32 strips in the x-direction and 32 strips in the y-direction with an active area of of 65.17 x 65.14 mm, such that each strip has a pitch of of $\sim$2 mm. This detector, with an α-particle detection efficiency of $\sim$50% is calibrated with a triple-α source (^{239}Pu, ^{241}Am, ^{244}Cm). In these experiments, the data acquisition was triggered by a charged particle event with an energy above $\sim$1 MeV. In order to obtain information on only the ions of interest, energy conditions were applied to the data, selecting only events associated with the α-decay of ^{151,152}Ho, given in Table 1.

Given the mass-resolution and size of the decay station detector, only $\sim$6 neighboring masses can be observed for a given measurement. Therefore, separate measurements were performed to investigate the quantities of Ho^+ bare ion and HoO^+

Table 1: Decay properties of pertinent holmium isotopes. Data from NNDC [27].

Isotope	Half-life (s)	α energy (MeV)	BR (%)
^{151}Ho	35.2(1)	4.522(22)	22(3)
^{151m}Ho	47.2(13)	4.610(22)	80(15)
^{152}Ho	161.8(3)	4.386(3)	12(3)
^{152m}Ho	50.0(4)	4.454(3)	10.8 (17)

molecular species for the different reaction conditions. In an effort to understand the different parameters and their effect on molecule formation, data were collected for 1 hr periods at different combinations of trapping time and gas flow rate. A 10 min decay period was observed prior to data collection, to ensure that any longer lived activity was fully decayed from the detector. Additionally, baseline measurements were performed, with no reactive gas flowing into the system, to look for any possible contaminants of similar mass already present in the system. For the observation of bare ion species, the spectrometer was tuned to center the $A/q = 151/1$, and for oxide species the spectrometer was tuned to $A/q = 167/1$. These measurements allow for the detection position, mass resolution, and mass dispersion of the molecular species to be determined in varying reaction conditions. Understanding any potential systematics in these values is critical for future low-statistics studies of SHE molecule formation.

3 Results

3.1 Baseline Measurements

Prior to adding O_2 gas to the system, baseline measurements were performed at the decay station to determine the quantities of Ho^+ bare ions available to react and whether or not any HoO^+ species were already present from reactions of Ho^+ with background contaminants, such as H_2O. The production of $^{151}Ho^+$ and $^{152}Ho^+$ was confirmed with A/q measurements at the decay station, where the detection position of the associated α decays of each isotope was performed. The decay properties of these isotopes are given in Table 1. An example decay station spectrum showing detection of the $^{151}Ho^+$ and $^{152}Ho^+$ ions is given in Figure 2(left).

In the baseline measurements performed looking for potential HoO^+ species, there was a clear presence of four species with $A/q = 167/1$, $168/1$, $169/1$ and $170/1$, shown in Figure 2(right). It is assumed that all of these species were produced with chemical reactions of Ho^+ with trace H_2O contamination within the system, which can form either $Ho(OH_2)^+$, $HoOH^+$, or HoO^+ species. Here, the $A/q = 167/1$ species is assigned as $^{151}HoO^+$, the $A/q = 168/1$ species are likely a combination of $^{152}HoO^+$ and $^{151}HoOH^+$, the $A/q = 169/1$ species are likely a combination of $^{152}HoOH^+$ and $^{151}Ho(H_2O)^+$, and the $A/q = 170/1$ species is assigned as $^{152}Ho(H_2O)^+$.

The H_2O pressure in the trap was observed to be consistent over time when comparing the RGA data for the "with gas" to the "no gas" baseline measurements. Therefore, the presence of the species within the oxide baseline measurements was treated as a background that could be corrected for. Baseline measurements were performed with the use of both the 50 and 100 ms trapping times. These background

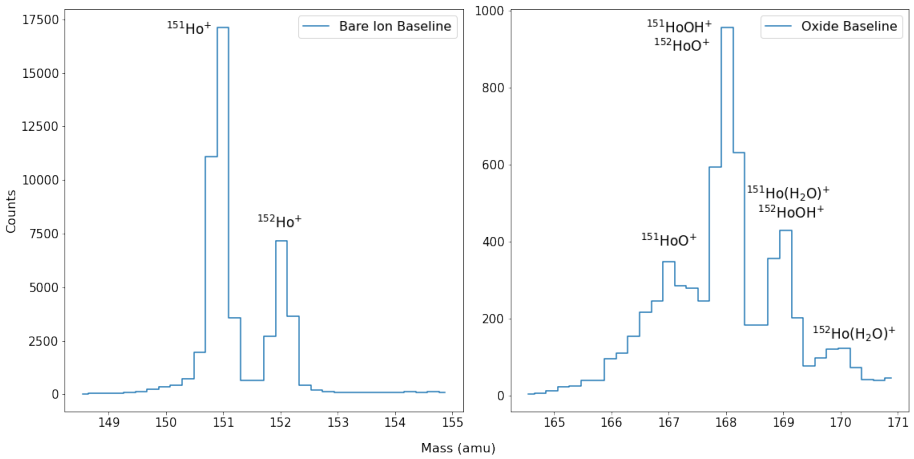

Fig. 2: Baseline measurements taken at the FIONA focal plane in the mass regimes of the ^{151,152}Ho bare ion (left) and oxide (right) species prior to O_2 gas being introduced. Here, the x-axis is the detection position scaled by the mass-dispersion to show the corresponding A/q being detected.

data were then subtracted from data taken with gas flowing, each normalized to the corresponding Rutherford rate to account for any inconsistencies in the production of Ho^+ ions between measurements. A sample result of this process, for data taken utilizing a 50 ms trapping time, is shown in Figure 3. After the subtraction, only peaks corresponding to the production of $^{151}HoO^+$ and $^{152}HoO^+$ molecules are present. The success of this background-subtraction method allowed for the data to then be further analyzed to investigate the kinetics of the HoO^+ formation from controlled exposure of Ho^+ to O_2.

3.2 Production of HoO^+

To produce the molecular species HoO^+, the Ho^+ ions were exposed to O_2 gas while contained within the RFQ trap. This chemical reaction was studied at three flow rates of O_2 gas, 5×10^{-5}, 1×10^{-4} and 5×10^{-4} mbarL/s. These flow rates are set with the use of a mass-flow controller. Additionally, each flow rate was examined at two trapping times, 50 and 100 ms. For each trapping time and flow rate combination, two decay station measurements were performed, one to observe the numbers of produced HoO^+ molecules and another to observe the remaining numbers of unreacted Ho^+ ions. The spectra of HoO^+ species detected were background subtracted to exclude molecules formed with the background H_2O contamination, as was discussed in the previous section.

The experimental data for the numbers of observed Ho^+ and HoO^+ ions taken at the different flow rates and trapping times of 50 and 100 ms are shown in Figures 4 and 5, respectively. In these figures, the numbers of bare Ho^+ ions observed at each of the three gas flow rates are shown in the top three histograms and the background corrected HoO^+ spectra are presented in the bottom three histograms. These data

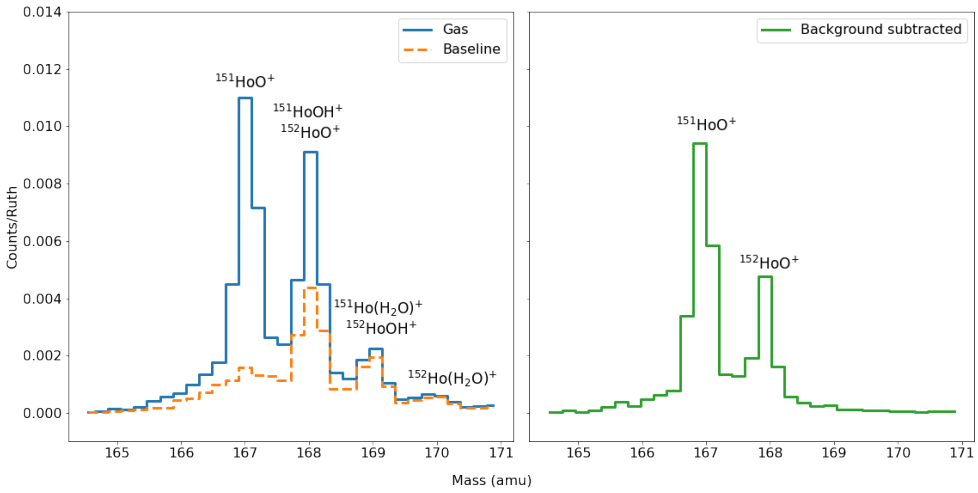

Fig. 3: The background subtraction technique and its results.(left) Comparison between data collected with no oxygen gas in the system, the "baseline" data (dashed line) and data collected with 1×10^{-5} mbarL/s of oxygen flowing into the trap, the "gas" data (solid line). (right) Data resulting from the subtraction of the baseline from the gas data shown on the left, attributed solely to the presence of reactions between holmium ions and oxygen gas. Here, the x-axis is the detection position scaled by the mass-dispersion to show the corresponding A/q being detected.

were fit with Gaussian distributions to determine the peak areas, the Full-Width at Half-Maximum (FWHM) and the position of the peaks. It is evident that as more O_2 is flowing through the trap, the observed amounts of $^{151,152}Ho^+$ bare ions decrease while the observed amounts of the associated oxide species increase, indicating that the chemical reaction did proceed.

3.3 Determination of Rate Constants

The chemical reaction studied here was previously investigated with stable Ho species [18]. There, it was determined the reaction proceeded via pseudo-first order kinetics with a reaction rate constant of k = 2.4(7) x 10^{-10} cm^3 molecule^{-1} s^{-1}. Here, different combinations of trapping times (t_{trap}) and gas flow rates ($[O_2]_{flow}$) were use to observe the production rate of HoO^+ formation in varied O_2 exposure within FIONA. The relative number of interactions between Ho^+ ions and O_2 molecules within the RFQ trap can be given as $t_{trap}[O_2]_{flow}$. However, it is possible to determine the true concentration of O_2 with the use of a calibration factor f, where $[O_2]_{true} = f[O_2]_{flow}$. Here, $[O_2]_{flow}$ is treated as a unit-less representation of the relative amount of O_2 within the trapping volume and f has pressure units of molecules/cm^3.

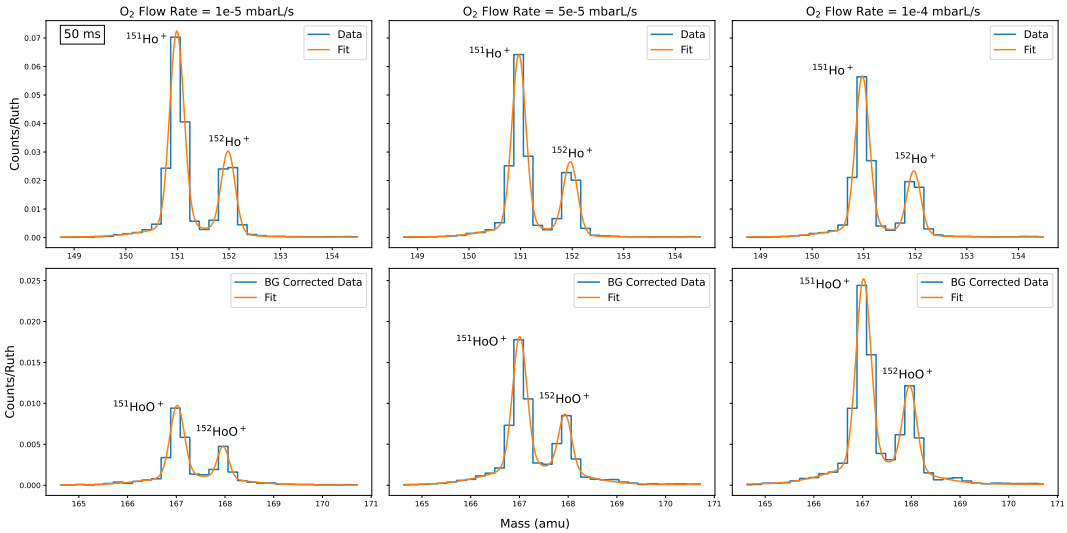

Fig. 4: Data collected for the 50 ms trapping time, depicted as counts per Rutherford event as a function of x-strip number. (Top) The fitted data collected for a mass-to-charge ratio of $A/q = 151/1$, showing the presence of ^{151,152}Ho$^+$. (Bottom) The fitted data collected for a mass-to-charge ratio of $A/q = 167/1$, showing the presence of various species associated with the holmium oxide and holmium hydroxide masses.

The pseudo-first order kinetics for the consumption of ^{151,152}Ho$^+$ and the production of ^{151,152}HoO$^+$, respectively can be described with Eqs. 2 and 3.

$$N_r(t) = \frac{R_r}{kf[\mathrm{O_2}]_{flow}}(1 - e^{-kf[\mathrm{O_2}]_{flow}t_{\mathrm{trap}}}) \tag{2}$$

$$N_p(t) = R_r t_{\mathrm{trap}} + R_p t_{\mathrm{trap}} - \frac{R_r}{kf[\mathrm{O_2}]_{flow}}(1 - e^{-kf[\mathrm{O_2}]_{flow}t_{\mathrm{trap}}}) \tag{3}$$

Here, $N_r(t)$ and $N_p(t)$ are the number of ions of reactant (^{151,152}Ho$^+$) and product (^{151,152}HoO$^+$) ions contained within the RFQ trap at a time t, respectively. R_r and R_p are the rates of reactant and product ions entering the trap every second, respectively. The reaction rate constant is given as k with units of cm^3 molecule^{-1} s^{-1} and f is the previously described calibration factor. The combined kinetic behavior of $N_r(t)$ and $N_p(t)$ can be described with Eq. (4).

$$\frac{N_p}{N_r + N_p} = 1 - \frac{N_r}{N_r + N_p} = 1 - \frac{R_r}{R_r + R_p}\frac{1}{kf[\mathrm{O_2}]_{flow}t_{\mathrm{trap}}}(1 - e^{-kf[\mathrm{O_2}]_{flow}t_{\mathrm{trap}}}) \tag{4}$$

Here, the ratios $\frac{N_p}{N_r+N_p}$ and $\frac{N_r}{N_r+N_p}$ are bound between 0 and 1.

Reaction rate curves were constructed from the experimental data by plotting the fraction to the total for both the bare ions remaining and the oxides species formed

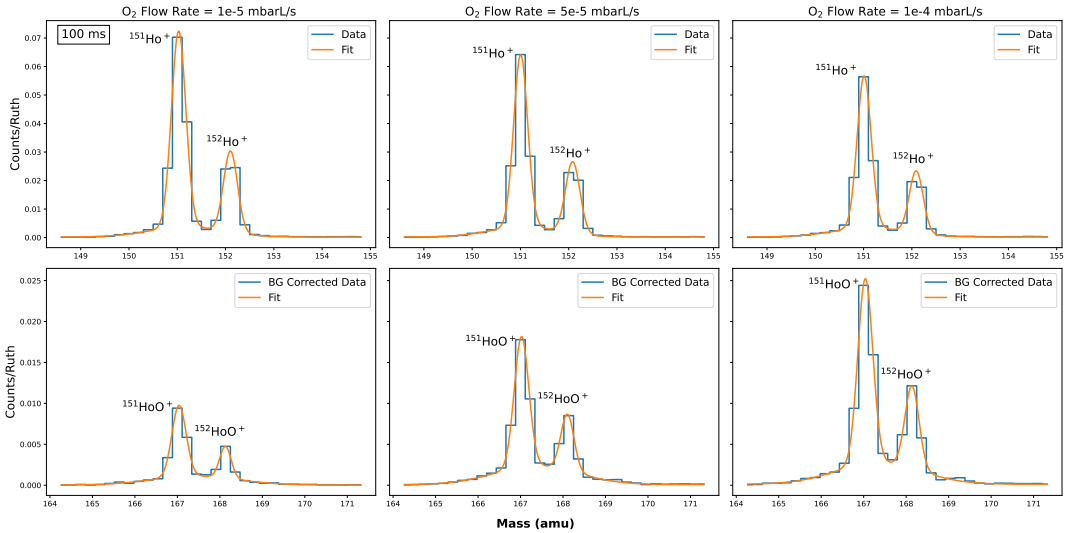

Fig. 5: Data collected for the 100 ms trapping time, depicted as counts per Rutherford event as a function of x-strip number. (Top) The fitted data collected for a mass-to-charge ratio of $A/q = 151/1$, showing the presence of $^{151,152}Ho^{+}$. (Bottom) The fitted data collected for a mass-to-charge ratio of $A/q = 167/1$, showing the presence of various species associated with the holmium oxide masses.

at given experimental conditions, as a function of $t_{trap}[O_2]_{flow}$. The rate curves were prepared separately for both the ^{151}Ho and ^{152}Ho species, and are shown in Figure 6. These were fit with a least-squares method according to Eqn. 4 to extract kf, the product of the reaction rate k and the calibration factor f. As is shown in Fig. 6, kf was found to be $1.1(2)\times10^{-5}$ s^{-1} and $1.1(3)\times10^{-5}$ s^{-1} for the production of $^{151}HoO^{+}$ and $^{151}HoO^{+}$, respectively. Given that k was previously measured to be $2.4(7)\times10^{-10}$ cm^3 molecule^{-1} s^{-1} [18], f could be readily determined and was found to be $4.6(15)\times10^{14}$ molecules/cm^3 and $4.6(19)\times10^{14}$ molecules/cm^3, for $^{151}Ho^{+}$ and $^{152}Ho^{+}$, respectively.

In the future, if it were desirable to measure the reaction rate for the formation of a SHE oxide from interactions of SHE ions with O_2, it would be necessary to also measure the "relative" reaction rate constant kf with FIONA for an element that has already been studied to react with O_2, such as Ho. As was shown here, the calibration factor f can be extracted by normalizing the observed reaction rate constant of the calibration element to the literature value. Then, f can be used to normalize the observed relative SHE reaction rate constant, determining k from kf. Note that this calibration factor is used solely to determine the effective pressure of the FIONA RFQ trap and does not assume any chemical similarities between the lighter homologue and the studied SHE. The procedure was carried out previously with FIONA to determine the reaction rate for the reduction of Lr^{2+} ions when exposed to O_2, where the measured reaction rate for the $^{151}Ho^{+} + O_2$ chemical reaction was observed to normalize and determine f [23].

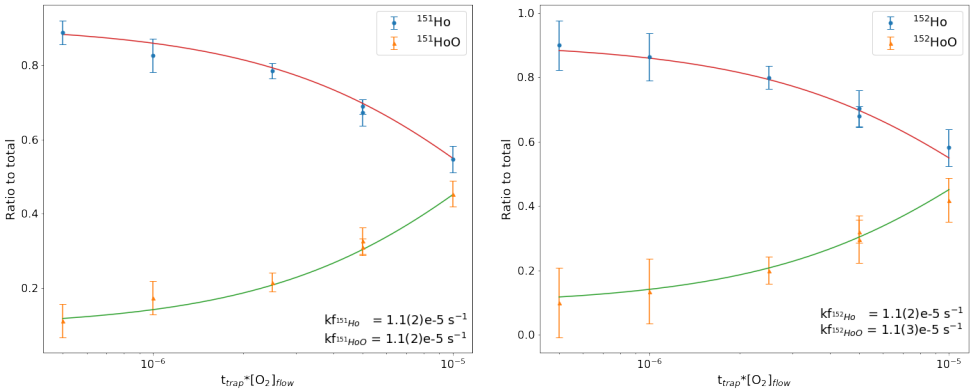

Fig. 6: Fits to the decrease of bare ion species and increase of oxides species as there is more opportunity for reactions with O_2 gas. The ratio of each of the species to the total is plotted as function of $t_{trap}[O_2]_{flow}$, where $[O_2]_{flow}$ is treated as a unit-less representation of the relative amount of O_2 within the trapping volume. For $^{151}Ho^+$ and $^{151}HoO^+$ species (left), the kf factor was fit to be $1.1(2)\times10^{-5}$ for both. For the $^{152}Ho^+$ and $^{152}HoO^+$ species (right), kf factor was fit to be $1.1(2)\times10^{-5}$ and $1.1(3)\times10^{-5}$, respectively.

3.4 FIONA Performance and Stability for Molecular Species Measurements

In looking towards low-satistics studies of SHE molecule formation, it is important that the detection positions and widths (FWHM) of A/q distributions be predictable. This enables low numbers of events to accurately be assigned an A/q value. Generally, FIONA measurements require initial optimizations to fine-tune the transmission, optics, mass resolution of the detected A/q distributions, and the mass dispersion (i.e., the shift in detection positions between adjacent A/q distributions per percentage difference in A/q). These optimizations are carried out using species with well-characterized masses that can be produced at high rates [26]. Once optimized, the FIONA settings can be extrapolated to study other A/q distributions of interest. The procedure involves scaling FIONA's electrostatic elements so that ions of the target A/q species follow the same trajectory as the calibration A/q species, ultimately reaching the same detection position. Details of this scaling procedure are provided in Ref. [21]. Knowing the mass dispersion then allows for the determination of A/q values for any neighboring distributions detected on either side of the calibrated position. In looking to perform low-statistics measurements of molecular species, it is necessary to confirm that this optimization procedure remains valid for different experimental conditions. To that end, this study collected high-statistics data to compare the detection positions, mass resolutions, and mass dispersions of Ho^+ and HoO^+ species in different experimental conditions.

In this experiment, FIONA was initially optimized for the detection of the $^{151}Ho^+$ and $^{152}Ho^+$ ions. Then, FIONA was scaled from $A/q = 151/1$ to $A/q = 167/1$

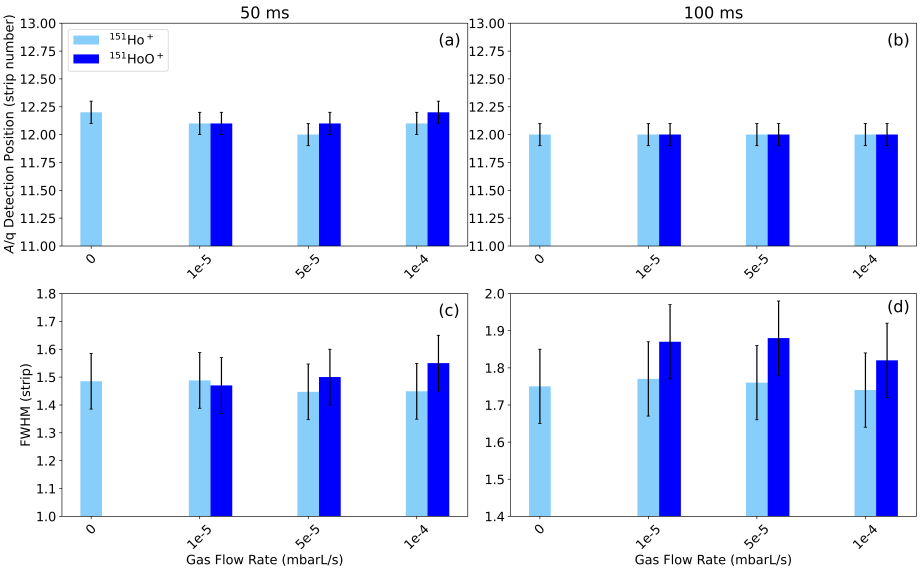

Fig. 7: The detection position and width (FWHM) of $^{151}HoO^+$ species compared to that of the $^{151}Ho^+$ species for different experimental conditions. (a-b) The detection position of $^{151}HoO^+$ species compared to the calibration position of $^{151}Ho^+$ species for trapping times of 50 ms and 100 ms, respectively. (c-d) The FWHM of the $A/q = 167/1$ $^{151}HoO^+$ distribution compared to the $A/q = 151/1$ $^{151}Ho^+$ species for trapping times of 50 ms and 100 ms, respectively.

such that the $^{151}HoO^+$ molecular species would be detected in the same position as the $^{151}Ho^+$ ions. The detection positions and mass resolutions (FWHM) of detected $^{151}Ho^+$ and $^{151}HoO^+$ species are shown in Figure 7 and for all combinations of experimental conditions (i.e. trapping times and gas flow rates). A Monte Carlo simulation was used to determine a systematic error for the detection positions and FWHM considering the statisitics and peak shapes observed here distributed across integer bins representative of the detector strips. The determined error for the detection position was 0.1 strips and for the FWHM was 0.2 strips. As shown in Figure 7(a-b) the $A/q = 167/1$ $^{151}HoO^+$ molecular species were consistently detected in the same position as the $A/q = 151/1$ $^{151}Ho^+$ bare ion species for all experimental conditions. Additionally, as can be seen in Figure 7(c-d), the observed FWHM for both species were also observed to be consistent for the differing gas flow rates for each trapping time. Note that the difference in FWHM in comparing the 50 ms and 100 ms measurements was due to a retune of FIONA between measurements. These measurements show that the expected detection position and mass resolution of molecular species are consistent with and can be predicted from those of bare ion species.

For a given FIONA tune, the mass dispersion is established during the initial optimization measurements. Here, the observed mass dispersion between the detection distributions of bare ions $^{151}Ho^+$ and $^{152}Ho^+$ was measured and compared to that

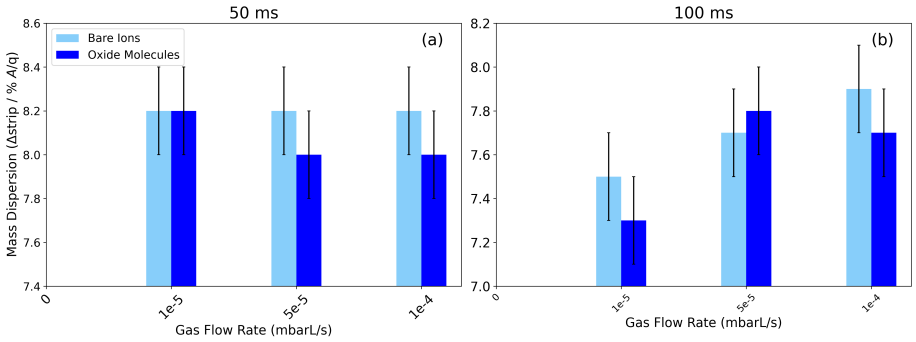

Fig. 8: The observed mass dispersion of molecular species as compared to the bare ion species at trapping times of 50 ms (a) and 100 ms (b), respectively.

of the molecular species $^{151}HoO^+$ and $^{152}HoO^+$ under various experimental conditions. As shown in Figure 8, the mass dispersion was consistent for both bare ions and molecular species, at approximately 8 strips per $\%\Delta A/q$, across all conditions. This consistency in mass dispersion for molecular species enables the determination of A/q for any observed species. These results demonstrate that the expected detection position, mass resolution, and mass dispersion are preserved whether bare ions or molecular species are being transported and detected. The predictability of A/q positions and widths, established by a high-statistics optimization, confirms that FIONA is well-suited for future low-statistics SHE experiments.

4 An outlook for the future of SHE chemistry

It has been demonstrated here that it is possible to produce and identify molecules for elements produced one-atom-at-a-time in nuclear reactions. The stability and consistency of measurements observed here for the formation of HoO^+ molecular species give confidence that this technique can be used for studies of SHE. It is anticipated that the dramatic impact of relativistic effects on the chemical properties of SHE will cause them to exhibit behaviors different than their lighter homologues. This means that their current placement on the periodic table of elements is likely not indicative of their chemical properties. To date the measurements performed on SHE from ion exchange, liquid-liquid extraction, and gas chromatography have laid an important groundwork in exploring their chemical properties. However, for continued progress, we need more advanced experimental techniques, such as what is presented here. The ability to directly identify and quantify SHE molecules formed in a chemical reactions opens the door for exciting future research in SHE chemistry.

The next generation of SHE research presents an opportunity to reevaluate how SHEs are positioned on the periodic table. An element's placement on the table provides a framework for understanding its chemical behavior, but it's understood that this placement can't capture every nuance of its reactivity. Given the challenges of experimentally studying SHEs, it's currently not possible to fully characterize their chemical properties. Therefore, it's crucial to carefully decide which properties are

most relevant for determining their placement. Most chemists today would likely argue that a modern periodic table should be organized by electronic structure, a concept that wasn't available to Mendeleev when he created his table. However, the predicted changes in electronic orbitals for SHEs and beyond complicate this approach. Some theorists have proposed rearranging some elements out of proton number order [28] or even using a three-dimensional periodic table to address this issue [29]. However, even if it is not obvious how rearrangements could be made to reflect the deviating chemical properties of SHE and beyond, discussions of rearrangement are ongoing. For example, the recent experimental confirmation that Lr ($Z = 103$) has a $7p^1$ as opposed to a $6d^1$ electronic configuration [30] has sparked renewed debate over the composition of Group 3 [31]. Moving forward, as new experimental data on these elements becomes available, these discussions should continue.

Direct observations of SHE molecule formation can offer two key insights on their electronic structure that can inform their appropriate placement. First, these studies can identify *preferred oxidation states* by determining how many ligands each element tends to bind. Confirming the preferred oxidation states of SHEs directly reflects their the underlying electronic structures and reactivity patterns. Experiments can be performed with FIONA, where SHE ions are reacted with fluorinating gases to produce fluoride molecular ions. Previous gas-phase studies of transition metals and lanthanides at room temperature have observed distributions of fluoride ions that correspond to the highest normally accessible oxidation state [32]. Furthermore, the distribution patterns of fluoride ions observed among different metal ions have been shown to reflect their distinct electronic configurations and sequential ionization potentials. Similar experiments can be performed with SHEs using FIONA to gain insight into their electronic structures.

Second, observation of molecule formation provides a means to probe the energetic accessibility of *"characteristic" valence electron configurations* that are directly associated with specific periodic table positions. Early SHEs occupy the d-block of the periodic table, and their chemical behavior should reflect the filling and reactivity of d orbitals. Based on their positions, the chemistry of Rf ($Z = 104$) is expected to correspond to the reactivity of a d^2 electron configuration, while Db ($Z = 105$) should correspond to that of a d^3 configuration. Given the production rates of Rf [4] and Db [33], we would expect to see ∼60 and ∼8 events per hour with FIONA, respectively, assuming a beam intensity of 1 pμA. These rates are three and four orders of magnitudes less than the production of ^{151,152}Ho in this study. SHE measurements would need to be performed for multiple hours with FIONA for identification of molecular species. However, these measurements are feasible given the results presented here. Previous gas-phase chemistry experiments have established mechanisms for chemical reactions that can identify the accessibility of d^1, d^2, and d^3 electron configurations based on the observed production of specific molecular species [34]. Determination of reaction constants for the formation of these molecules could yield even more precise information on the energies of these characteristic ground states as was done previously for Ho [18]. A re-investigation of SHE periodic table placement could begin by targeting these chemical reactions and examining whether specific molecular species are formed.

5 Conclusions

To date, no molecular species of SHEs have been directly identified, highlighting the need for innovative experimental techniques to advance the field. A novel gas-phase chemistry technique developed at LBNL has opened the door to the next generation of SHE research. In this study, it was demonstrated that the technique presented successfully produced HoO^+ molecules from reactions of Ho^+, created one-atom-at-a-time in nuclear reactions, with controlled exposure to O_2 gas. Measurements at varying trapping times and gas flow rates determined the reaction rate and assessed the stability of molecule identifications using FIONA, based on comparisons of positions and widths of A/q distributions. These results establish that this approach is well-suited for low-statistics studies of SHEs, demonstrating the power and functionality of the BGS and FIONA system for advancing SHE chemistry.

The ability to directly observe molecular species can provide key insights into the oxidation states and electronic configurations of SHEs, critical for refining our understanding of their fundamental chemistry. This knowledge could prompt a reevaluation of the placement of SHEs on the periodic table by offering a more detailed picture of their chemical behavior. FIONA's unique capabilities will be instrumental in advancing the study of chemistry at the boundaries of the periodic table.

Acknowledgements
The authors acknowledge the operations staff of the 88" cyclotron facility at Lawrence Berkeley National Laboratory for providing the ^{40}Ar beam necessary for this work.
Funding This material is based upon work supported by the U.S. Department of Energy, Office of Science, Office of Nuclear Physics under contract DE-AC02-05CH11231 and Lawrence Berkeley National Laboratory's Laboratory Directed Research and Development Program. The work at Lawrence Livermore National Laboratory is performed under the auspices of the U.S. Department of Energy under Contract DE-AC52-07NA27344 (MAS). Partial support was provided by the U.S. Department of Energy, Office of Science, Basic Energy Sciences, Division of Chemistry, Biosciences and Geosciences, Heavy Element Chemistry Program under Contract DE-AC02-05CH11231 at LBNL (JLP, JMG, AD, JKG, ZS, DKS).

Declarations

Conflict of Interest All authors declare that they have no conflicts of interest.

References

[1] Smits, O. R., Düllmann, C. E., Indelicato, P., Nazarewicz, W. & Schwerdtfeger, P. The quest for superheavy elements and the limit of the periodic table. *Nature Reviews Physics* **2**, 515–531 (2020). https://doi.org/10.1038/s42254-020-0227-9.

[2] Pershina, V. Electronic structure and properties of superheavy elements. *Nuclear Physics A* **944**, 578–613 (2015). https://doi.org/10.1016.j.nuclphysa.2015.04.007.

[3] Pershina, V. Relativity in the electronic structure of the heaviest elements and its influence on periodicities in properties. *Radiochimica Acta* **107**, 833–863 (2019). https://doi.org/10.1515/ract-2018-3098.

[4] Dragojević, I., Gregorich, K. E., Düllmann, C. E., Garcia, M. A., Gates, J. M., Nelson, S. L., Stavsetra, L., Sudowe, R. & Nitsche, H. Influence of projectile neutron number in the ^{208}Pb(^{48}Ti, n)^{255}Rf and ^{208}Pb(^{50}Ti, n)^{257}Rf reactions. *Phys. Rev. C* **78**, 024605 (2008). https://doi.org/10.1103/PhysRevC.78.024605.

[5] Oganessian, Y. T., others, Lobanov, Y. V., Abdullin, F. S., Polyakov, A. N., Sagaidak, R. N., Shirokovsky, I. V., Tsyganov, Y. S., Voinov, A. A., Gulbekian, G. G. & Bogomolov, S. L. Synthesis of the isotopes of elements 118 and 116 in the ^{249}Cf and ^{245}Cm $+^{48}$ Ca fusion reactions. *Phys. Rev. C* **74**, 044602 (2006). https://doi.org/10.1103/PhysRevC.74.044602.

[6] Schädel, M. & Shaughnessy, D. (eds) *The Chemistry of Superheavy Elements* (Springer-Verlag, Berlin, Heidelberg, 2014).

[7] Even, J., others, Düllmann, C. E., Haba, H., Asai, M., Sato, T. K., Brand, H., Nitto, A. D., Eichler, R., Fan, F. L. *et al.* Synthesis and detection of a seaborgium carbonyl complex. *Science* **345**, 1491–1493 (2014). https://doi.org/10.1126/science.1255720.

[8] Düllmann, C. E., others, Dressler, R., Eberhardt, K., Eichler, B., Eichler, R., Gäggeler, H. W., Ginter, T. N., Glaus, F., Gregorich, K. E. *et al.* Chemical investigation of hassium (element 108). *Nature* **418**, 859–862 (2002). https://doi.org/10.1038/nature00980.

[9] Eichler, R., others, Albin, Y. V., Belozerov, A. V., Bozhikov, G. A., Chepigin, V. I., Dmitriev, S. N., Dressler, R., Gäggeler, H. W., Gorshkov, V. A. *et al.* Indication for a volatile element 114. *Radiochimica Acta* **98**, 133–139 (2010). https://doi.org/10.1524/ract.2010.1705.

[10] Yakushev, A., others, Türler, A., Schädel, M., Düllmann, C. E., Ackermann, D., Andersson, L.-L., Block, M., Brüchle, W., Dvorak, J. *et al.* Superheavy element flerovium (element 114) is a volatile metal. *Inorganic Chemistry* **53**, 1624–1629 (2014). https://doi.org/10.1021/ic4026766.

[11] Yakushev, A., others, Düllmann, C. E., Khuyagbaatar, J., Jäger, E., Krier, J., Runke, J., Albers, H. M., Asai, M., Block, M. & Despotopulos, J. On the adsorption and reactivity of element 114, flerovium. *Frontiers in Chemistry* **10**, 01–11 (2022). https://doi.org/10.3389/fchem.2022.976635.

[12] Armentrout, P. B. & Baer, T. Gas-phase ion dynamics and chemistry. *Journal of Physical Chemistry* **100**, 12866–12886 (1996). https://doi.org/10.1021/jp953478a.

[13] Schwarz, H. Relativistic effects in gas-phase ion chemistry: An experimentalist's view. *Angewandte Chemie International Edition* **42**, 4442–4454 (2003). https://doi.org/10.1002/anie.200301651.

[14] Armentrout, P. B. Periodic trends in gas-phase oxidation and hydrogenation reactions of lanthanides and 5d transition metal cations. *Mass Spectrometry Reviews* **41**, 606–626 (2022). https://doi.org/10.1002/mas.21703.

[15] Gibson, J. K. Gas-phase chemistry of actinide ions: probing the distinctive character of the 5f elements. *International Journal of Mass Spectrometry* **214**, 1–21 (2002). https://doi.org/10.1016/S1387-3806(01)00559-0.

[16] Gibson, J. K. & Marçalo, J. New developments in gas-phase actinide ion chemistry. *Coordination Chemistry Reviews* **250**, 776–783 (2006). https://doi.org/10.

1016/j.ccr.2005.09.011, actinide Chemistry.
[17] Svanberg, S. *Atomic and Molecular Spectroscopy* (Springer, 2001).
[18] Koyanagi, G. K. & Bohme, D. K. Oxidation reactions of lanthanide cations with N_2O and O_2: Periodicities in reactivity. *J. Phys. Chem. A* **105**, 8964–8968 (2001). https://doi.org/10.1021/jp011627m.
[19] Gurell, J., Wahlgren, G. M., Nave, G. & Wyart, J.-F. Wavelengths, energy levels and hyperfine structure constants in Ho ii. *Physica Scripta* **79**, 035306 (2009). https://doi.org/10.1088/0031-8949/79/03/035306, published 3 March 2009.
[20] Gregorich, K. E. Simulation of recoil trajectories in gas-filled magnetic separators. *Nuc Instrum. Meth. A* **711**, 47–59 (2013). https://doi.org/https://doi.org/10.1016/j.nima.2013.01.020.
[21] Gates, J. M. & Pore, J. L. Studies of heavy and super heavy elements with FIONA: the broad impact of mass-number idenfitications. *Eur. Phys. L. A* **58**, 196 (2022). https://doi.org/10.1140/epja/s10050-022-00844-1.
[22] Kwarsick, J. T., Pore, J. L., Gates, J. M., Gregorich, K. E., Gibson, J. K., Jian, J., Pang, G. K. & Shuh, D. K. Assessment of the second-ionization potential of lawrencium: Investigating the end of the actinide series with a one-atom-at-a-time gas-phase ion chemistry technique. *The Journal of Physical Chemistry A* **125**, 6818–6828 (2021). https://doi.org/10.1021/acs.jpca.1c01961.
[23] Kwarsick, J. Assessment of the second-ionization potential of lawrencium: Investigating the end of the actinide series with a one-atom-at-a-time gas-phase ion chemistry technique. *J. Phys. Chem. A* **125**, 6818–6828 (2021). https://doi.org/10.1021/acs.jpca.1c01961.
[24] Gates, J. M., others, Rudolph, D., Appleton, C., Barrios, B. M., Benitez, J. Y., Bordeau, M., Botha, W., Campbell, C. M., Chadderton, J. *et al.* Toward the discovery of new elements: Production of livermorium ($z = 116$) with ^{50}Ti. *Phys. Rev. Lett.* **133**, 172502 (2024). https://doi.org/10.1103/PhysRevLett.133.172502.
[25] Xie, Z. Q. & Lyneis, C. M. Performance of the upgraded LBNL AECR ion source. Tech. Rep., LBNL (1997).
[26] Gates, J. M. Prospects of A and Z identification experiments at LBNL. *EPJ Web Conf.* **131**, 08003 (2016).
[27] National Nuclear Data Center, B. N. L. Nudat (nuclear structure and decay data) (2008).
[28] Pyykkö, P. A suggested periodic table up to z 172, based on dirac–fock calculations on atoms and ions. *Physical Chemistry Chemical Physics* **13**, 161–168 (2011). https://doi.org/10.1039/C0CP01575J.
[29] Nefedov, V., Trzhaskovskaya, M. & Yarzhemskii, V. Electronic configurations and the periodic table for superheavy elements. *Doklady Physical Chemistry* **408(2)**, 159–151 (2006).
[30] Sato, T., others, Borschevsky, A., Stora, T., Sato, N., Kaneya, Y., Tsukada, K., Düllmann, C. E., Eberhardt, K., Eliav, E. *et al.* Measurement of the first ionization potential of lawrencium, element 103. *Nature* **520**, 209–211 (2015). https://doi.org/10.1038/nature14342.
[31] Scerri, E. Provisional report on discussions on group 3 of the periodic table. *Chemistry International* **43**, 31–34 (2021). https://doi.org/10.1515/ci-2021-0115.

[32] Gibson, J. K. Transition-metal fluoride ions, MFn+, from gas-phase reactions of nascent laser-ablated M+ with fluorocarbons. *Journal of Fluorine Chemistry* **78**, 65–74 (1996). https://doi.org/10.1016/0022-1139(96)03414-8.

[33] Gates, J. M., others, Gregorich, K. E., Dragojević, I., Düllmann, C. E., Ellison, P. A., Folden III, C. M., Garcia, M. A., Stavsetra, L., Sudowe, R. & Hoffman, D. C. Comparison of reactions for the production of ^{258,257}Db: ^{208}Pb(^{51}V, xn) and ^{209}Bi(^{50}Ti, xn). *Phys. Rev. C* **78**, 034604 (2008). https://doi.org/10.1103/PhysRevC.78.034604.

[34] Marçalo, J., Santos, M. & Gibson, J. K. Gas-phase reactions of doubly charged actinide cations with alkanes and alkenes—probing the chemical activity of 5f electrons from Th to Cm. *Physical Chemistry Chemical Physics* **13**, 18322–18329 (2011). https://doi.org/10.1039/C1CP21399G.

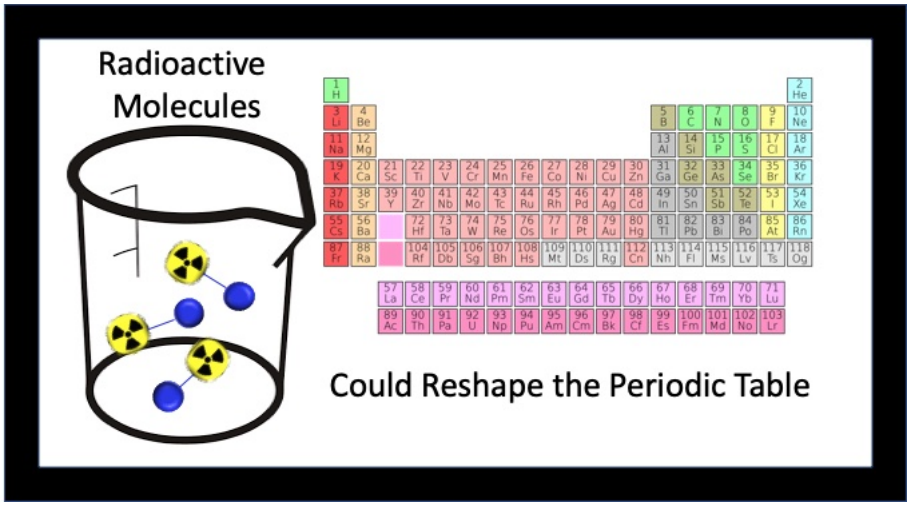

Fig. 9: TOC Graphic